Kinetics and Catalysis, Vol. 46, No. 6, 2005, pp. 884–890. Translated from Kinetika i Kataliz, Vol. 46, No. 6, 2005, pp. 932–939.
Original Russian Text Copyright © 2005 by Turko, Ivanova, Plyasova, Litvak, Rogov.

Synthesis and Characterization of Fluorite-Like Ce–Zr–Y–La–O Systems

G. A. Turko, A. S. Ivanova, L. M. Plyasova, G. S. Litvak, and V. A. Rogov

Boreskov Institute of Catalysis, Siberian Branch, Russian Academy of Sciences, Novosibirsk, 630090 Russia

Received July 14, 2004

Abstract—Ce–Zr–O and Ce–Zr–Y–La–O materials obtained under various conditions and at varying component ratios are characterized. At Ce/Zr ≈ 1, a tetragonal phase that can hardly be distinguished from a cubic phase by X-ray diffraction forms in the ternary system. Raising the precipitation temperature favors the formation of two-phase systems. Promoting the Ce/Zr = 0.26–0.62 materials with both yttrium and lanthanum favors the formation of a single-phase specimen, namely, a (Ce, Zr, Y, La)O_2 fluorite-like solid solution at 600°C. This structure persists up to 1150°C. The specific surface area of the (Ce, Zr, Y, La)O_2 materials is primarily determined by their calcination temperature: S_{sp} = 50–80 m^2/g at 600°C and 0.6–0.8 m^2/g at 1150°C. The specimens calcined at 600°C are mesoporous, with uniformly sized pores of mean diameter 32 ± 2 Å, and have no micropores. According to TPR data, the specimens calcined at 600°C are reduced with hydrogen in two steps that can apparently be interpreted as surface and bulk reduction. The Ce/Zr = 0.26 and 0.40 specimens calcined at 1150°C are reduced in a single step, giving rise to TPR peaks at 707 and 686°C, respectively, and their degree of reduction increases with decreasing Ce/Zr.

Three-way catalysts (TWCs) of composition NM/$Ce_{1-x}Zr_xO_{2-x}$/support (NM = noble metal) for the simultaneous removal of hydrocarbons, carbon monoxide, and nitrogen oxides from the exhaust gas of automobile engines have been widely used since the 1980s [1]. The working conditions of TWCs are very different from those of most industrial catalysts [2], because the initial air–fuel ratio varies as the engine is operated. Therefore, TWCs must be able to compensate for the changes in the exhaust composition. This requirement is satisfied by the cerium–zirconium oxide system, which is the most important component of TWCs. According to the present views [3], the Ce–Zr–O component plays the following roles:

(1) It makes possible oxidation–reduction cycles at a varying air–fuel ratio owing to the presence of the Ce^{4+}/Ce^{3+} redox couple.

(2) It affords more oxygen vacancies than CeO_2, retaining its fluorite structure.

(3) It stabilizes the particle size of the noble metal present in the TWC.

The oxygen vacancy fraction and the total oxygen storage capacity of $Ce_{0.63}Zr_{0.37}O_2$ are reported to be ~4 times higher that those of CeO_2 [4]. As a rule, the highest oxygen storage capacity is shown by $Ce_{1-x}Zr_xO_{2-x}$ with x = 0.2–0.4 [4]. The latest trend has been toward a lower CeO_2 content of the cerium–zirconium component. However, this raises the problem of conserving and stabilizing the fluorite structure. A stabilizing effect can be exerted by alkaline- and rare-earth ions [2].

Here, we report the preparation and physicochemical properties of a thermally stable single-phase cerium–zirconium oxide with a fluorite structure stabilized by yttrium and lanthanum cations.

EXPERIMENTAL

The specimens to be examined were obtained as follows. An aqueous solution containing metal nitrates in an appropriate ratio was treated with aqueous ammonia at a prescribed pH and temperature. The resulting suspension was filtered, and the cake was washed with distilled water until the washings were free of nitrate ions. Next, the solid was dried in air and then in an oven at 110°C for 12 h. The resulting material was heat-treated at 600–700°C in flowing dry air for 2–4 h and calcined in a muffle furnace at 900–1150°C for 4–12 h.

The main components of the oxides thus prepared were quantified by atomic absorption spectroscopy [5]. Thermal analysis was performed in air using Q1500D and DTG-60H (Shimadzu) thermoanalytical systems. The sample weight was 500 mg (Q1500D) or 40 mg (DTG-60H). The samples were examined between room temperature (18–21°C) and 1200°C at a heating rate of 10 K/min. Temperature was measured with an accuracy of ±5 K; weight loss, with an accuracy of ±1%.

X-ray diffraction was carried out on a URD-63 diffractometer using graphite-monochromated CuK_α radiation and a reflected-beam technique. Diffraction patterns were recorded in the point scanning mode at a 2θ of 10° to 70°–90°, a scanning pitch of τ = 0.05°, and a data collection time of 5 s at each point. The diffraction patterns were processed using the PCW.2.4, Origin, and

0023-1584/05/4606-0884 © 2005 MAIK "Nauka/Interperiodica"

Polikristall programs [6, 7]. Phase analysis was carried out by comparing the observed diffraction patterns with theoretical diffraction patterns for known structures taken from the ICDS data base [8], using the PCW.2.4 program and taking into account the profiles of the diffraction peaks. The peak profiles were described by the PsevdoViot2 function, which is the superposition of the Lorentzian function $y = 1/(1 + kx^2)^2$ and the Gaussian function $y = \exp(-kx^2)$ [9]. Profile parameters were refined up to the best possible fit between the calculated and observed profiles. The degree of coincidence between the calculated and observed data was evaluated in terms of the divergence factor R_d throughout the diffraction pattern. After the profile parameters had been refined, it was possible to determine the integrated intensities and integrated halfwidths of the diffraction peaks. For two-phase samples, it was possible to estimate, from the integrated intensity data, the volume or weight percentages of the phases with an accuracy of 2–5%, depending on the amounts and particle size of the phases. By analysis of the angular dependence of the integrated peak width for $\sin\theta/\lambda$ reflections of two or more orders, using an approximation method [10, 11], we separated the broadening effects due to the particle size and microdistortions. Microstructure parameters were mainly determined along the [111] direction. The unit cell parameters of the phases were refined by the least-squares processing of d_{hkl} data using the Polikristall and PCW.2.4 programs. The latter was used for all samples for the reason that it provided close fits and allowed a quicker integrated characterization of the sample, including semiquantitative phase analysis and the determination of unit cell parameters, the size of the coherently scattering region, and the degree of microdistortion. The unit cell parameters were used to determine the cationic composition of the cerium–zirconium phases. These phases were fluorite-like substitutional solid solutions, either cubic or tetragonal, depending on their composition. According to Vegard's rule [12], the unit cell parameters of a substitutional solid solution are nearly linear functions of composition since they depend on the ionic radius of the substituting component. For cubic solid solutions, the unit cell parameter of pure CeO_2 was taken from ICSD (no. 72155) [8]. The room-temperature parameter a for pure ZrO_2 viewed as a cubic structure was derived from the unit cell volume of the monoclinic phase (ICSD, no. 80042 [8]), which is stable at room temperature. For tetragonal solid solutions, the initial unit cell parameters were those of the terminal compositions $Ce_{0.12}Zr_{0.88}O_2$ [13] and $Ce_{0.5}Zr_{0.5}O_2$ [14]. At an error of Δa = 0.002–0.005 Å in the unit cell parameters, the Ce/Zr ratio was determined with an accuracy of 1–2%.

Specific surface area was determined by thermal argon desorption [15] with an error of ±10%. Texture parameters were derived from low-temperature (–196°C) nitrogen adsorption isotherms recorded using an ASAP-2400 instrument (Micrometrics).

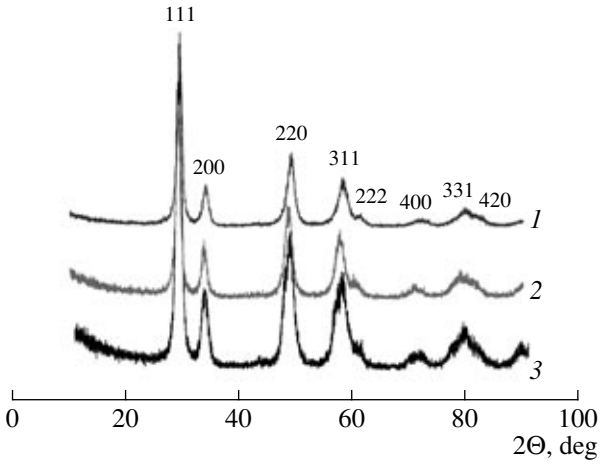

Fig. 1. X-ray diffraction patterns from cerium–zirconium oxides precipitated at (*1*, *2*) 20 and (*3*) 70°C and calcined at 900°C. Ce/Zr = (*1*) 0.66, (*2*) 1.08, and (*3*) 1.17.

Temperature-programmed reduction (TPR) with hydrogen was carried out in a flow reactor between room temperature and 900°C at a heating rate of 10 K/min. The concentration of hydrogen in argon was 10 vol %, and the gas flow rate was 40 ml/min. The resulting water was frozen out at –80°C. Hydrogen concentration was controlled with a flowmeter. The size of catalyst pellets was 0.25–0.50 mm, and the catalyst sample weight was 0.2 g. Prior to measurements, the samples were conditioned in oxygen at 500°C for 5 h.

RESULTS AND DISCUSSION

$Ce_{1-x}Zr_xO_{2-x}$ system. The diffraction patterns recorded for samples calcined at 900°C are shown in Fig. 1, and the profile analysis of one of these patterns is presented in Fig. 2. The most important characteristics of the phases examined are listed in Table 1. Clearly, only the two specimens precipitated at room temperature are single phases. Both can be assigned to either a cubic or tetragonal structure, since the tetragonal distortion is small (a/c = 0.97 for specimen 1 and 0.99 for specimen 2). These data are consistent with earlier results indicating that, at Ce/Zr ≈ 1, the oxide phase is tetragonal and is almost indistinguishable by X-ray diffraction from the cubic phase [16, 17]. The Ce/Zr values derived from the tetragonal unit cell data are in close agreement with the actual chemical compositions of these specimens. Raising the precipitation temperature to 70°C results in a two-phase specimen consisting of a cubic phase with a high ceria content ($Ce_{1-x}Zr_xO_{2-x}$, x = 0.20–0.27) and a phase that can be indexed in two ways, as in the case of the single-phase specimens. Assigning the second phase to a tetragonal structure leads to a smaller R_d factor and to a better agreement between the observed and calculated Ce/Zr values.

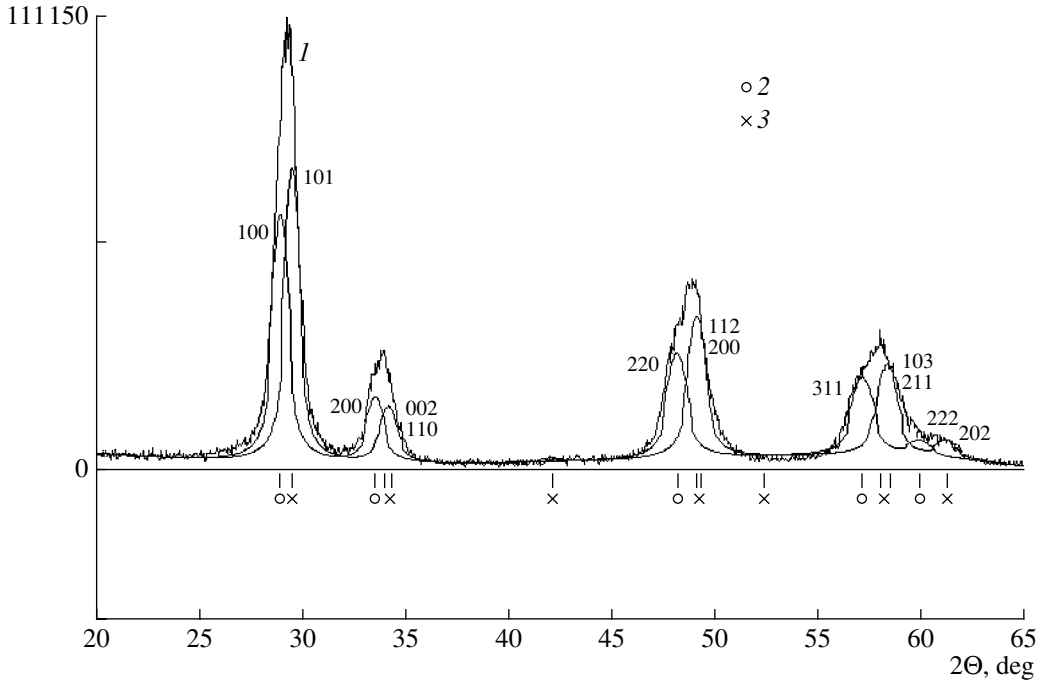

Fig. 2. X-ray diffraction patterns (*1*) recorded for cerium–zirconium oxide with Ce/Zr = 1.08 calcined at 900°C and (*2*, *3*) calculated for (*2*) cubic $Ce_{0.78}Zr_{0.22}O_2$ and (*3*) tetragonal $Ce_{0.37}Zr_{0.66}O_2$.

The specimens calcined at 700°C have similar specific surface areas, regardless of their synthesis conditions and Ce/Zr ratio (Table 1). The specimens calcined at 900°C have a much smaller specific surface area.

Thus, cerium–zirconium oxides with Ce/Zr ≈ 1 can be either single- or two-phase, depending on synthesis conditions. Raising the zirconium content results in the formation of a tetragonal solid solution and in a decrease in thermal stability. Therefore, it is necessary to stabilize the cubic structure of the cerium–zirconium solid solution. The yttrium and lanthanum cations are candidate stabilizers.

Ce–Zr–Y–La–O system. According to thermoanalytical data (Fig. 3), the samples of this system exhibit similar thermal behaviors: their DTA curves show endothermic peaks at 120–175°C due to the loss of physically adsorbed water and exotherms at 335 ± 5 and 385–480°C. Note that the temperature of the first

Table 1. Properties of $Ce_{1-x}Zr_xO_{2-x}$ oxides

Specimen no.	Composition	Precipitation temperature, °C	Phase composition (900°C)*	R_d	*a*/*c*	Refined compositions of the phases	S_{sp}, m^2/g	
							700°C	900°C
1	$Ce_{0.40}Zr_{0.60}O_2$	20	100% cub.	16.34	–	$Ce_{0.51}Zr_{0.49}$	58	0.02
			100% tetr.	13.58	0.97	$Ce_{0.46}Zr_{0.54}$		
2	$Ce_{0.52}Zr_{0.48}O_2$	20	100% cub.	16.83	–	$Ce_{0.66}Zr_{0.34}$	52	0.04
			100% tetr.	16.35	0.99	$Ce_{0.49}Zr_{0.51}$		
3	$Ce_{0.54}Zr_{0.46}O_2$	70	15.0% cub.	16.64	–	$Ce_{0.85}Zr_{0.15}$	57	6.5
			85.0% tetr.			$Ce_{0.56}Zr_{0.44}$		
			32.7% cub.	10.40	0.99	$Ce_{0.78}Zr_{0.22}$		
			67.3% tetr.			$Ce_{0.37}Zr_{0.63}$		

Note: cub. = cubic; tetr. = tetragonal.
* The calcination temperature is 900°C.

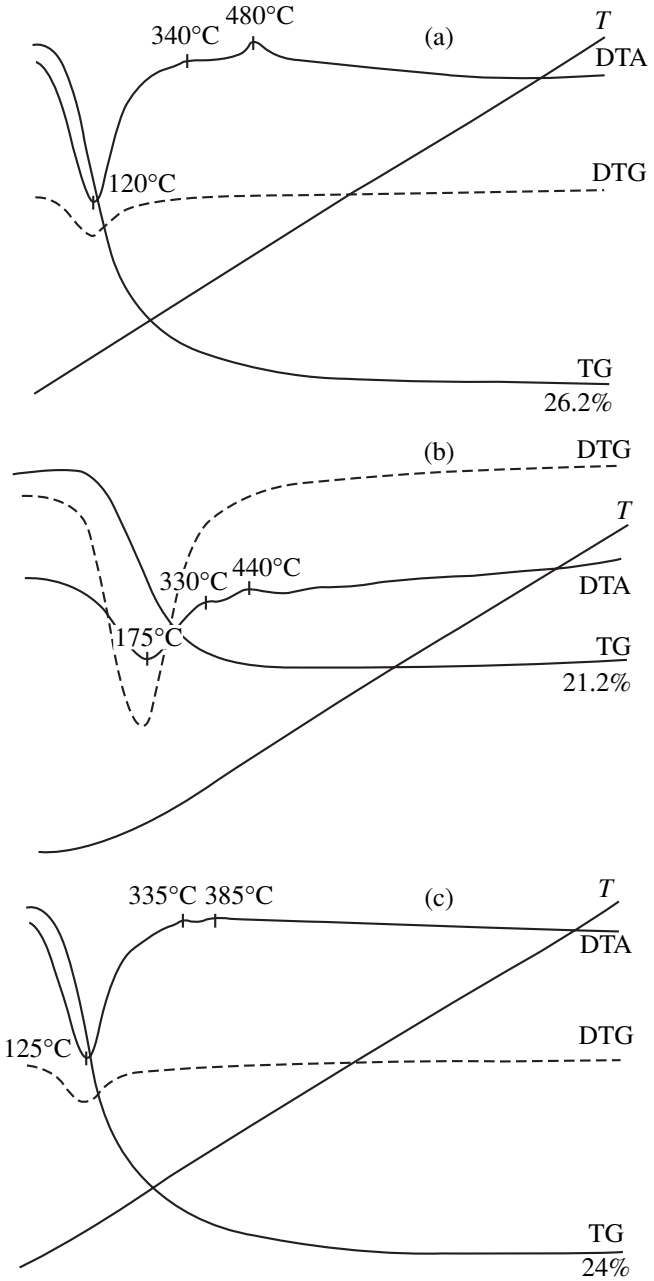

Fig. 3. Thermoanalytical curves for
(a) $Ce_{0.18}Zr_{0.69}Y_{0.09}La_{0.04}O_{1.935}$,
(b) $Ce_{0.31}Zr_{0.58}Y_{0.06}La_{0.05}O_{1.946}$, and
(c) $Ce_{0.33}Zr_{0.53}Y_{0.10}La_{0.04}O_{1.930}$.

exotherm (335 ± 5°C) is invariable and is composition-independent, while the temperature of the second exotherm, which is 385°C for $Ce_{0.33}Zr_{0.53}Y_{0.10}La_{0.04}O_{1.930}$ and 480°C for $Ce_{0.18}Zr_{0.69}Y_{0.09}La_{0.04}O_{1.935}$, grows with increasing zirconium content. Introducing 10 mol % CeO_2 or La_2O_3 into zirconium dioxide was reported to give rise to an exotherm at 440 and 675°C, respectively, because of the formation of a solid solution based on cubic zirconium dioxide [18]. It is believed that the exotherms observed in this study are also due to the formation of a solid solution. Further raising the temperature does not bring about any other thermal events. All of the specimens show similar total weight losses of about 24 ± 2%. Thus, the thermoanalytical data suggest that the phase transitions in this multicomponent oxide system are complete at ~500°C.

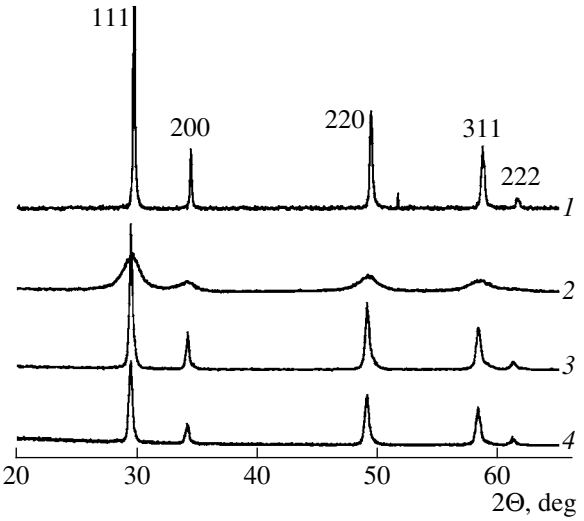

Fig. 4. X-ray diffraction patterns from (*1*) $Ce_{0.18}Zn_{0.69}Y_{0.09}La_{0.04}O_{1.935}$ calcined at 1150°C, (*2*) $Ce_{0.26}Zr_{0.65}Y_{0.06}La_{0.03}O_{1.954}$ calcined at 600°C, (*3*) $Ce_{0.26}Zr_{0.65}Y_{0.06}La_{0.03}O_{1.954}$ calcined at 1150°C, and (*4*) $Ce_{0.31}Zr_{0.58}Y_{0.06}La_{0.05}O_{1.946}$ calcined at 1150°C.

The X-ray diffraction patterns from specimens calcined at 600 and 1150°C are presented in Fig. 4. The reflections from the specimen calcined at 600°C (curve *2*) are broad, indicating a low degree of crystallinity and a small particle size. The specimens calcined at 1150°C are characterized by sharper reflections (curves *1*, *3*, *4*) and, therefore, have a higher degree of crystallinity (Table 2). The totality of observed reflections are consistent with the fluorite-like cubic structure characteristic of CeO_2 and the cubic modification of ZrO_2. The unit cell parameters of the phases examined fall between the unit cell parameters of these oxides (Table 2), suggesting that the phases are solid solutions. However, these parameters do not point to the actual Ce/Zr ratios, because they are altered by the La and Y ions present in these solid solutions. It is clear from the data listed in Table 2 that the unit cell parameter increases with an increasing cerium dioxide content of the solid solution and is independent of calcination temperature within the measurement error ($\Delta a \sim 0.01$ Å at 600°C and $\Delta a \sim 0.001$ Å at 1150°C).

The crystallite size (D) and microdistortion ($\Delta d/d$) of the solid solutions are determined by the calcination temperature (Table 2). For example, D is 40–70 Å at 600°C and ~1000 Å at 1150°C. These data are in agreement with adsorption data.

The specific surface area of the Ce–Zr–Y–La–O specimens calcined at 600°C is 50–80 m^2/g (Table 3),

Table 2. Phase composition and structure parameters of Ce–Zr–Y–La–O phases calcined at 600 and 1150°C

Composition	Phase		a, Å		D_{111}, Å		$\Delta d/d$	
	600°C	1150°C	600°C	1150°C	600°C	1150°C	600°C	1150°C
$Ce_{0.18}Zr_{0.69}Y_{0.09}La_{0.04}O_{1.935}$	Fluorite-like cubic		5.217	5.214	55	≈1000	0.0029	0.0023
$Ce_{0.26}Zr_{0.65}Y_{0.06}La_{0.03}O_{1.954}$			5.230	5.227	70	≈1000	0.0036	0.0026
$Ce_{0.31}Zr_{0.58}Y_{0.06}La_{0.05}O_{1.946}$			–	5.230	–	≈1000	–	0.0030
$Ce_{0.33}Zr_{0.53}Y_{0.10}La_{0.04}O_{1.930}$			5.268	–	40	–	0.0041	–

Table 3. Texture parameters of Ce–Zr–Y–La–O phases calcined at 600 and 1150°C

No.	Composition	S_{sp}, m^2/g		Low-temperature N_2 adsorption*		
		600°C	1150°C	S_{sp}, m^2/g	V_{por}, cm^3/g	$D_{av.por}$, Å
1	$Ce_{0.18}Zr_{0.69}Y_{0.09}La_{0.04}O_{1.935}$	53	0.8	52.2	0.039	29.7
2	$Ce_{0.26}Zr_{0.65}Y_{0.06}La_{0.03}O_{1.954}$	71	0.8	–	–	–
3	$Ce_{0.31}Zr_{0.58}Y_{0.06}La_{0.05}O_{1.946}$	80	0.6	–	–	–
4	$Ce_{0.33}Zr_{0.53}Y_{0.10}La_{0.04}O_{1.930}$	61	–	64.4	0.054	33.4

* For specimens calcined at 600°C.

in agreement with earlier data [19]. Heat treatment at 1150°C dramatically reduces the specific surface area to 0.6–0.8 m^2/g. However, this value is about one order of magnitude larger that the specific surface area of unpromoted cerium–zirconium oxides calcined at 900°C (Table 1).

A typical nitrogen adsorption isotherm is plotted in Fig. 5a, and the volumetric pore-size distribution derived from this isotherm for the Ce/Zr specimen calcined at 600°C is shown in Fig. 5b. The low-temperature nitrogen adsorption data are presented in Table 3. The specific surface areas derived from the nitrogen adsorption data are nearly equal to those derived from argon desorption data (Table 3). The phases examined are mesoporous, with uniformly sized pores. Their specific pore volume (V_{por}) is 0.039–0.054 cm^3/g, their

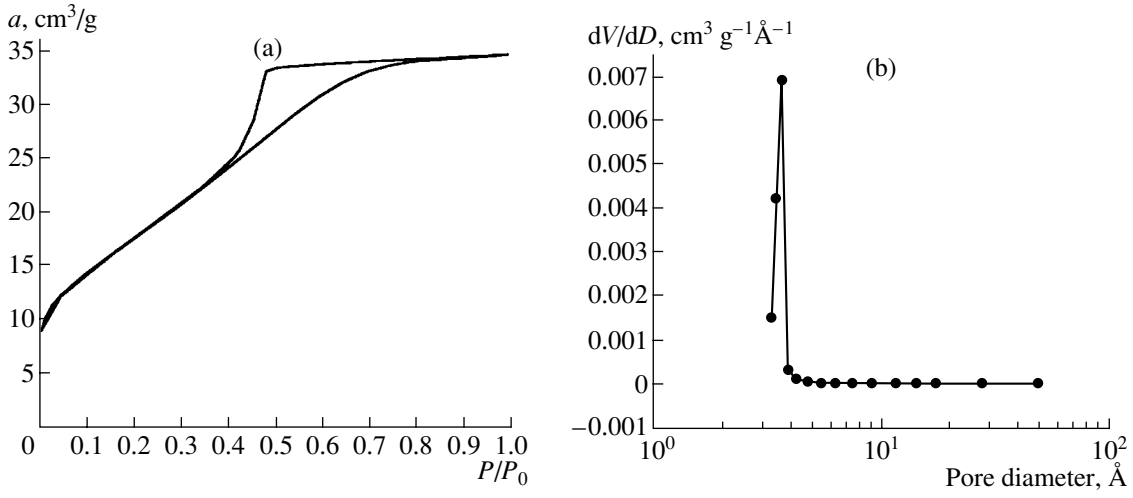

Fig. 5. (a) Nitrogen adsorption isotherm and (b) volumetric pore-size distribution for $Ce_{0.33}Zr_{0.53}Y_{0.10}La_{0.04}O_{1.930}$ calcined at 600°C.

Table 4. Effects of the composition and calcination temperature of Ce–Zr–Y–La–O phases on their reduction behavior

Composition	Ce/Zr	T_{calc}, °C	T_{red}, °C	H_2 uptake, mmol/g		Degree of reduction
				observed	calculated	
$Ce_{0.18}Zr_{0.69}Y_{0.09}La_{0.04}O_{1.935}$	0.26	600	599, 749	1.03	0.69	1.49
$Ce_{0.26}Zr_{0.65}Y_{0.06}La_{0.03}O_{1.954}$	0.40	600	582, 716	1.05	0.95	1.11
$Ce_{0.31}Zr_{0.58}Y_{0.06}La_{0.05}O_{1.946}$	0.54	600	584, 703	1.08	1.11	0.97
$Ce_{0.33}Zr_{0.53}Y_{0.10}La_{0.04}O_{1.930}$	0.62	600	656, 850	1.31	1.13	1.16
$Ce_{0.18}Zr_{0.69}Y_{0.09}La_{0.04}O_{1.935}$	0.26	1150	707	0.63	0.69	0.91
$Ce_{0.26}Zr_{0.65}Y_{0.06}La_{0.03}O_{1.954}$	0.40	1150	686	0.81	0.95	0.85
$Ce_{0.31}Zr_{0.58}Y_{0.06}La_{0.05}O_{1.946}$	0.54	1150	691, 760	0.87	1.11	0.78

mean pore diameter (D_{por}) is 32 ± 2 Å, and they have no micropores.

In order to determine the reduction sequence for the phases, we carried out the temperature-programmed reduction (TPR) of the phases with hydrogen. The TPR spectra of the specimens calcined at 600°C have complicated shapes. These specimens are reduced in two steps, as follows from the presence of two peaks in each TPR curve. For Ce/Zr = 0.26, 0.40, 0.54, and 0.62, these peaks occur at 599 and 749, 582 and 716, 584 and 703, and 657 and 840°C, respectively (Table 4). According to earlier reports [20–22], the TPR spectrum of CeO_2 shows two peaks due to surface and bulk reduction (at ≈500 and ≈800°C, respectively). A similar reduction behavior is shown by $Ce_{0.1}Zr_{0.8}Y_{0.1}O_2$ [2]. Thus, the two reduction steps observed for the oxides considered can also be surface reduction and bulk reduction.

The specimens calcined at 1150°C are characterized by another TPR profile (Fig. 6b): they are reduced in a single step, and their reduction peaks are weaker. For example, the Ce/Zr = 0.26 and 0.40 specimens are reduced in one step, giving rise to peaks at 707 and 686°C, respectively (Table 4). These temperatures are intermediate between the step I and step II reduction temperatures of the specimens calcined at 600°C. The Ce/Zr = 0.54 specimen is characterized by two peaks occurring at 691 and 760°C (Fig. 6b, curve *3*; Table 4). Therefore, the higher the cerium dioxide content the higher the reduction temperature.

As follows from the equation $2CeO_2 + H_2 \longrightarrow Ce_2O_3 + H_2O$, 2.91 mmol of H_2 is required for the

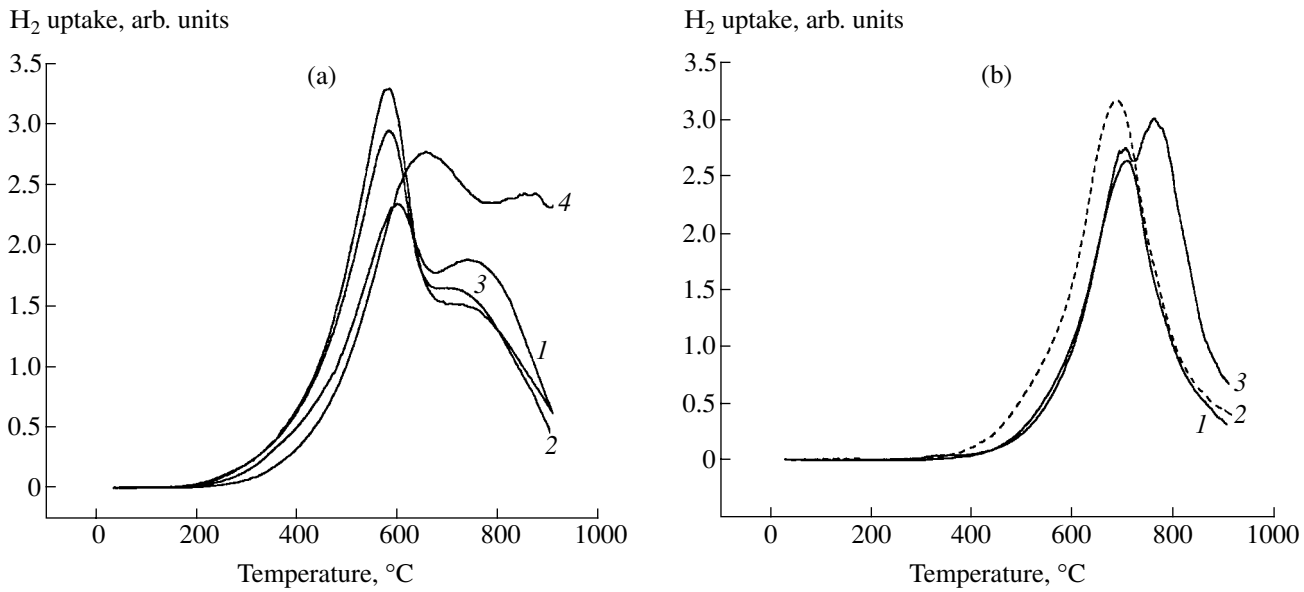

Fig. 6. TPR profiles for specimens calcined at (a) 600 and (b) 1150°C: (*1*) $Ce_{0.18}Zr_{0.69}Y_{0.09}La_{0.04}O_{1.935}$, (*2*) $Ce_{0.26}Zr_{0.65}Y_{0.06}La_{0.03}O_{1.954}$, and (*3*) $Ce_{0.31}Zr_{0.58}Y_{0.06}La_{0.05}O_{1.946}$, and (*4*) $Ce_{0.33}Zr_{0.53}Y_{0.10}La_{0.04}O_{1.930}$.

reduction of 1 g of CeO_2. This value was used to calculate the amounts of hydrogen necessary for the reduction of the CeO_2 in the specimens examined. Evidently, in the TPR of specimens calcined at 600°C, the observed hydrogen uptake increases with increasing Ce/Zr (Table 4). For all specimens but the Ce/Zr = 0.54 phase, the observed hydrogen uptake exceeds the calculated value and, accordingly, the degree of reduction is above unity. A plausible explanation of this finding is that, in the specimens calcined at 600°C, the state of the surface components is composition-dependent and it is surface reduction that is responsible for the variation of the degree of reduction.

This effect is not observed for the specimens calcined at 1150°C (Table 4). Raising the calcination temperature causes a decrease in the amount of hydrogen necessary for the reduction of a given composition. Note also that the degree of reduction of the phases calcined at 1150°C increases with decreasing Ce/Zr (Table 4).

According to Fornasiero *et al.* [23], total hydrogen consumption is a measure of the relative amount of oxygen that is thermodynamically available at a given temperature. This amount is conventionally termed total oxygen storage capacity. Since an increase in the degree of reduction signifies an intensification of oxygen transfer in solid solutions based on cerium and zirconium dioxides, the above data suggest that catalysts based on the Ce–Zr–Y–La–O system with Ce/Zr = 0.26–0.40 will be very efficient.

REFERENCES

1. Trovarelli, A., de Leitenburg, C., Boaro, M., and Dolcetti, G., *Catal. Today*, 1999, vol. 50, p. 353.
2. Kulyova, S.P., Lunina, E.V., Lunin, V.V., Kostyuk, B.G., Muravyova, G.P., Kharlanov, A.N., Zhilinskaya, E.A., and Aboukais, A., *Chem. Mater.*, 2001, vol. 13, p. 1491.
3. Rao, G.R., Kaspar, J., Meriani, S., Di Monte, R., and Graziani, M., *Catal. Lett.*, 1994, vol. 24, p. 107.
4. Madier, Y. and Descorme, C., Le Govic, A.M., and Duprez, D., *J. Phys. Chem. B*, 1999, vol. 103, p. 10999.
5. Price, W.J., *Analytical Atomic Absorption Spectrometry*, London: Heyden, 1972.
6. Kraus, W. and Nolze, G., *CPD Newsletter*, 1998, vol. 20, p. 27.
7. Solov'eva, L.P., Tsybulya, S.V., and Zabolotnyi, V.A., *Polikristall—sistema programm dlya strukturnykh raschetov* (Polikristall Program Package for Structure Calculations), Novosibirsk: Inst. Kataliza, 1988.
8. ICSD, code 72155, 754478, 80042.
9. Langford, J.I., *J. Appl. Crystallogr.*, 1978, vol. 1, p. 22.
10. Williamson, G.K. and Hall, W.H., *Acta Metall.*, 1953, vol. 1, p. 43.
11. Iveronova, V.I. and Revkevich, G.P., *Teoriya rasseyaniya rentgenovskikh luchei* (Theory of X-ray Beam Scattering), Moscow: Mosk. Gos. Univ., 1978.
12. Guinier, A., *Théorie et technique de la radiocristallographie*, Paris: Dunod, 1956.
13. ICSD, code 75470.
14. JCPDS, 38-1436.
15. Buyanova, N.E., Karnaukhov, A.P., and Alabuzhev, Yu.A., *Opredelenie udel'noi poverkhnosti dispersnykh i poristykh materialov* (Determination of the Specific Surface Area of Disperse Porous Materials), Novosibirsk: Inst. Kataliza, 1978.
16. Bozo, C., Gaillard, F., and Guilhaume, N., *Appl. Catal., A*, 2001, vol. 220, p. 69.
17. Vlaic, G., Di Monte, R., Fornasiero, P., Fonda, E., Kaspar, J., and Graziani, M., *J. Catal.*, 1999, vol. 182, p. 378.
18. Ivanova, A.S., Moroz, E.M., and Litvak, G.S., *Kinet. Katal.*, 1992, vol. 33, nos. 5–6, p. 1208.
19. Mamontov, E., Egami, T., Brezny, R., Koranne, M., and Tyagi, S., *J. Phys. Chem.*, 2000, vol. 104, p. 11110.
20. Yao, H.C. and Yu, YaoY.F., *J. Catal.*, 1984, vol. 86, p. 254.
21. Trovarelli, A., *Catal. Rev.—Sci. Eng.*, 1996, vol. 38, p. 439.
22. Jen, H.-W., Graham, G.W., Chun, W., McCabe, R.W., Cuif, J.-P., Deutsch, S.E., and Touret, O., *Catal. Today*, 1999, vol. 50, p. 309.
23. Fornasiero, P., Di Monte, R., Rao, G.R., Kaspar, J., Meriani, S., Trovarelli, A., and Graziani, M., *J. Catal.*, 1995, vol. 151, p. 168.